

# General Green's-function formalism for transport calculations with *spd* Hamiltonians and giant magnetoresistance in Co- and Ni-based magnetic multilayers

S. Sanvito\* and C. J. Lambert†

*School of Physics and Chemistry, Lancaster University, LA1 4YB Lancaster, United Kingdom*

J. H. Jefferson

*DERA, Electronics Sector, Malvern, WR14 3PS Worcestershire, United Kingdom*

A. M. Bratkovsky‡

*Hewlett-Packard Laboratories, 3500 Deer Creek Road, Palo Alto, California 94304-1392*

(Received 26 August 1998)

A general Green's-function technique for elastic spin-dependent transport calculations is presented, which (i) scales linearly with system size and (ii) allows straightforward application to general tight-binding Hamiltonians (*spd* in the present work). The method is applied to studies of conductance and giant magnetoresistance (GMR) of magnetic multilayers in current perpendicular to planes geometry in the limit of large coherence length. The magnetic materials considered are Co and Ni, with various nonmagnetic materials from the 3*d*, 4*d*, and 5*d* transition metal series. Realistic tight-binding models for them have been constructed with the use of density functional calculations. We have identified three qualitatively different cases which depend on whether or not the bands (densities of states) of a nonmagnetic metal (i) form an almost perfect match with one of spin subbands of the magnetic metal (as in Cu/Co spin valves), (ii) have almost pure *sp* character at the Fermi level (e.g., Ag), and (iii) have almost pure *d* character at the Fermi energy (e.g., Pd, Pt). The key parameters which give rise to a large GMR ratio turn out to be (i) a strong spin polarization of the magnetic metal, (ii) a large energy offset between the conduction band of the nonmagnetic metal and one of spin subbands of the magnetic metal, and (iii) strong interband scattering in one of spin subbands of a magnetic metal. The present results show that GMR oscillates with variation of the thickness of either nonmagnetic or magnetic layers, as observed experimentally. [S0163-1829(99)03118-5]

## I. INTRODUCTION

The discovery<sup>1</sup> of giant magnetoresistance (GMR) in metallic multilayers about a decade ago has attracted a great deal of attention. This is not only because of the possibility of building sensitive magnetometers, but also because GMR provides valuable insight into spin-dependent transport in inhomogeneous systems. The GMR is the drastic change in electrical resistance that occurs when a strong magnetic field is applied to a superlattice made with alternating magnetic and nonmagnetic (spacer) metallic layers. Early experiments were conducted with the so-called current-in-plane (CIP) configuration, in which the current flows parallel to the plane of the layers. In this configuration the dimensions of the system are macroscopic with transport properties being reasonably described by a classical Boltzmann equation<sup>2</sup> and GMR is associated with the spin-dependent scattering of electrons at the interfaces.

The first experiments with the current perpendicular to the plane (CPP) of the layers<sup>3</sup> paved the way to a completely different regime, where quantum effects can play a dominant role. In good quality superlattices the elastic mean free path can extend over several layers and the spin diffusion length can be longer than the total superlattice thickness. In this case we can talk, according to Mott,<sup>4</sup> about majority and minority spin carriers as two independent spin fluids which remain coherent as they cross the superlattice layers. Then a

full quantum description is required. For such structures the magnetoconductance and GMR are found to be oscillatory functions of the nonmagnetic layer thickness<sup>5</sup> with periods extending over several atomic planes. This is due to a periodic switching of the exchange coupling from ferromagnetic to antiferromagnetic, as a function of a spacer layer thickness. In the former case the GMR effect vanishes. Despite the evidence of such important quantum effects, early theoretical work was based on spin-dependent scattering at interfaces and/or magnetic impurities and the effects of quantum interference have been usually ignored. In 1995 Schep, Kelly, and Bauer<sup>6,7</sup> challenged this conventional picture and showed that large values of GMR (of the order of 120%) can exist even in absence of impurity scattering.

The aim of the present paper is to develop a quantitative approach to quantum transport, which describes the dependence of GMR on specific materials and/or layer thicknesses. Our calculations are based on the Landauer-Büttiker formalism,<sup>8</sup> using a nearest-neighbor tight-binding *spd* Hamiltonian. The tight-binding energy parameters have been fitted to accurate *ab initio* density functional calculations.

We have developed and present here a completely general technique for calculating Green's functions and hence a scattering *S* matrix and transport coefficients of a finite superlattice connected to pure crystalline semi-infinite leads. This allowed us to perform a systematic study of Co/A and Ni/A

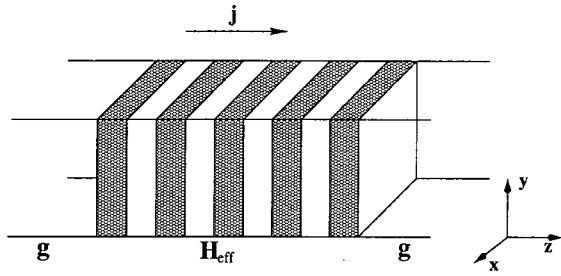


FIG. 1. Sketch of a finite superlattice connected to two semi-infinite leads.

multilayers, where  $A = \text{Cu, Ag, Pd, Au, and Pt}$ , and analyze optimal conditions for GMR.

We shall consider below a GMR ratio of a finite superlattice connected to two semi-infinite crystalline leads,<sup>9</sup> as sketched in Fig. 1. The GMR ratio is defined by

$$\text{GMR} = (\Gamma_{\text{FM}}^{\uparrow} + \Gamma_{\text{FM}}^{\downarrow} - 2\Gamma_{\text{AF}}^{\uparrow\downarrow}) / 2\Gamma_{\text{AF}}^{\uparrow\downarrow}, \quad (1.1)$$

where  $\Gamma_{\text{FM}}^{\sigma}$  is the conductance of a given spin channel  $\sigma$  in the ferromagnetic (FM) configuration and  $\Gamma_{\text{AF}}^{\uparrow\downarrow}$  is the corresponding conductance (for either spin) in the antiferromagnetic (AF) state. We calculate the conductance by evaluating the Landauer formula<sup>8</sup>

$$\Gamma^{\sigma} = \frac{e^2}{h} T^{\sigma}, \quad (1.2)$$

where  $T^{\sigma}$  is the total transmission coefficient for the spin  $\sigma$  calculated at the Fermi energy. Below we shall assume a perfect match at the interface between the fcc lattices of the different metals. This assumption is particularly good in the case of Co, Cu, and Ni, which have almost identical lattice constants. We shall consider below crystalline systems with smooth interfaces, where  $k_{\parallel}$  is a good quantum number (we use the symbol  $\parallel$  for the in-plane coordinates and  $\perp$  for the direction of the current). The Hamiltonian can then be diagonalized in the Bloch basis  $k_{\parallel}$  to yield

$$\Gamma^{\sigma} = \sum_{k_{\parallel}} \Gamma^{\sigma}(k_{\parallel}) = \frac{e^2}{h} \sum_{k_{\parallel}} T^{\sigma}(k_{\parallel}), \quad (1.3)$$

where the sum over  $k_{\parallel}$  is extended over the two-dimensional Brillouin zone in the case of infinite cross section and over the allowed discrete  $k_{\parallel}$ 's in the case of finite cross section. We note that equation (1.2) is valid in general, even in the presence of disorder. Nevertheless, from a computational point of view it requires the definition of a cell including all degrees of freedom of the scatterer, which rapidly leads to unmanageably large matrices. On the contrary, Eq. (1.3) is

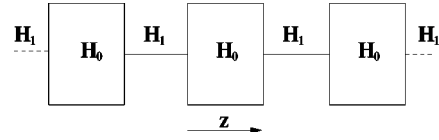


FIG. 2. An infinite system formed from periodically repeated slices.

limited to cases with translational invariance. However, disorder may be rather easily introduced even in these cases by using a sufficiently large unit cell and repeating it periodically. This standard supercell approach has been used, for instance, in Refs. 10 and 11 for the calculations of Co/Cu and Fe/Cr multilayers.

## II. GREEN'S-FUNCTION FORMALISM FOR SCATTERING MATRIX

The problem of analyzing a realistic tight-binding model with  $spd$  orbitals on each site represents a difficult numerical problem which requires various approximations.<sup>10-13</sup> Usually the studies are limited to  $1s$  band models,<sup>14,15</sup> with inclusion of spin splitting to mimic a spin-dependent transport.<sup>16,17</sup> In this section we describe a very general and efficient technique for calculating the  $S$  matrix and hence the transmission coefficients of an arbitrary scattering region such as a superlattice, attached to two semi-infinite crystalline leads. The key steps of the calculation are (i) the evaluation of the retarded Green's function  $g$  of the semi-infinite leads and (ii) the construction of an effective Hamiltonian  $H_{\text{eff}}$  describing the scattering region and its coupling to the leads. The approach described below provides a versatile method for computing these two entities, which are then combined via Dyson's equation to yield the Green's function of the whole structure, for which the transport coefficients are sought. A feature of the technique is that it avoids adding a small imaginary part to the energy and provides a semianalytic formula for  $g$ .

### A. The Green's function of an arbitrary semi-infinite lead

To compute the Green's function for a semi-infinite crystalline lead with a finite cross-section, we first calculate the Green's function of an infinite system and then derive it for the semi-infinite lead by applying boundary conditions at the end of the lead. To this end, we shall now consider the infinite system shown in Fig. 2.

If  $z$  is the direction of electron transport, the system comprises a periodic sequence of slices, described by an intraslice matrix  $H_0$ , coupled by a nearest-neighbor interslice hopping matrix  $H_1$ . The nature of the slices need not be specified at this stage. They can describe a single state atom in an atomic chain, or an atomic plane, or a more complex cell. For such a general system, the total Hamiltonian  $H$  can be written as an infinite matrix of the form

$$H = \begin{pmatrix} \dots & \dots \\ \dots & H_0 & H_1 & 0 & \dots & \dots & \dots & \dots \\ \dots & H_{-1} & H_0 & H_1 & 0 & \dots & \dots & \dots \\ \dots & 0 & H_{-1} & H_0 & H_1 & 0 & \dots & \dots \\ \dots & 0 & 0 & H_{-1} & H_0 & H_1 & 0 & \dots \\ \dots & \dots \\ \dots & \dots \end{pmatrix}, \quad (2.1)$$

where  $H_0$  is Hermitian and  $H_{-1} = H_1^\dagger$ . The Schrödinger equation for this system is of the form

$$H_0 \psi_z + H_1 \psi_{z+1} + H_{-1} \psi_{z-1} = E \psi_z, \quad (2.2)$$

where  $\psi_z$  is a column vector corresponding to the slice at the position  $z$  with  $z$  an integer measured in units of interslice distance. Let the quantum numbers, corresponding to the degrees of freedom within a slice, be  $\mu = 1, 2, \dots, M$  and the corresponding components of  $\psi_z$  be  $\psi_z^\mu$ . For example, in the following sections these will enumerate the atomic sites within the slice and the valence (*spd*-) orbitals on a site. The Schrödinger equation may then be solved by introducing the Bloch state

$$\psi_z = n_{k_\perp}^{1/2} e^{ik_\perp z} \phi_{k_\perp}, \quad (2.3)$$

where  $\phi_{k_\perp}$  is a normalized  $M$ -component column vector and  $n_{k_\perp}^{1/2}$  is the arbitrary constant. Substituting this into Eq. (2.2) gives

$$(H_0 + H_1 e^{ik_\perp} + H_{-1} e^{-ik_\perp} - E) \phi_{k_\perp} = 0. \quad (2.4)$$

Our goal is to compute the Green's function  $g$  of such a structure for all real energies. For a given energy  $E$ , one has to find all possible values (both real and complex) of the wave vectors  $k_\perp$  by solving the secular equation

$$\det(H_0 + H_1 \chi + H_{-1} / \chi - E) = 0, \quad (2.5)$$

where  $\chi = e^{ik_\perp}$ . In contrast with the conventional band theory, where the problem is to compute the  $M$  values of  $E$  for a given (real) choice of  $k_\perp$ , our aim is to compute the complex roots  $\chi$  of the polynomial (2.5) for a given (real) choice of  $E$ . Consider first the case where  $H_1$  is not singular. We note that for real  $k_\perp$ , conventional band theory yields  $M$  energy bands  $E_n(k_\perp)$ ,  $n = 1, \dots, M$ , with  $E_n(k_\perp + 2\pi) = E_n(k_\perp)$ . As a result, for any given  $E$  there exists a pair of solutions for  $k_\perp = k$ . For each real  $k$ , corresponding to a positive group velocity ("right-moving" solution)

$$v_k = \frac{1}{\hbar} \frac{\partial E(k)}{\partial k} > 0, \quad (2.6)$$

there exists a second ("left-moving") solution  $k_\perp = \bar{k}$  with the negative group velocity

$$v_{\bar{k}} = \frac{1}{\hbar} \frac{\partial E(\bar{k})}{\partial \bar{k}} < 0. \quad (2.7)$$

These real wave vectors define the open scattering channels of the structure and in the simplest case, where  $H_1 = H_{-1}$ , one finds  $k = -\bar{k}$ . All other solutions for  $k$  have finite imaginary parts and they would correspond to the closed channels in the leads. For each solution  $k_\perp$  the Hermitian conjugate of Eq. (2.4) shows that  $k_\perp^*$  is also a solution. Hence, to each "right-decaying" solution  $k$  having a positive imaginary part, there always exists a "left-decaying" solution  $\bar{k}$  with a negative imaginary part. For the purpose of constructing the Green's function we introduce a division of the roots of Eq. (2.4) into two sets: the first set of  $M$  wave vectors labeled  $k_l$  ( $l = 1, \dots, M$ ) correspond to right-moving and right-decaying plane waves and the second set labeled  $\bar{k}_l$  ( $l = 1, \dots, M$ ) corresponds to left-moving and left-decaying plane waves.

Although the solutions to Eq. (2.5) can be found by using a root tracking algorithm, for numerical purposes it is more convenient to map Eq. (2.4) onto an equivalent eigenvalue problem by introducing the matrix  $\mathcal{H}$

$$\mathcal{H} = \begin{pmatrix} -H_1^{-1}(H_0 - E) & -H_1^{-1}H_{-1} \\ \mathcal{I} & 0 \end{pmatrix}, \quad (2.8)$$

where  $\mathcal{I}$  is the  $M \times M$  unit matrix. The eigenvalues of  $\mathcal{H}$  are the  $2M$  roots  $e^{ik_l}, e^{i\bar{k}_l}$  and the upper  $M$  components of the eigenvectors of  $\mathcal{H}$  are the sought eigenvectors  $\phi_{k_l}, \phi_{\bar{k}_l}$ .

To construct the retarded Green's function  $g_{zz'}$  of an infinite lead, we note that, except at  $z = z'$ ,  $g$  is simply a wave function and hence must have the form

$$g_{zz'} = \begin{cases} \sum_{l=1}^M \phi_{k_l} e^{ik_l(z-z')} \mathbf{w}_{k_l}^\dagger, & z \geq z', \\ \sum_{l=1}^M \phi_{\bar{k}_l} e^{i\bar{k}_l(z-z')} \mathbf{w}_{\bar{k}_l}^\dagger, & z \leq z', \end{cases} \quad (2.9)$$

where the  $M$ -component vectors  $\mathbf{w}_{k_l}$  and  $\mathbf{w}_{\bar{k}_l}$  are to be determined. Since  $g_{zz'}$  is retarded both in  $z$  and  $z'$ , it satisfies the Green's function equation corresponding to Eq. (2.2) and is continuous at the point  $z = z'$ , so that one obtains

$$g_{zz'} = \begin{cases} \sum_{l=1}^M \phi_{k_l} e^{ik_l(z-z')} \bar{\phi}_{k_l}^\dagger \mathcal{Y}^{-1}, & z \geq z', \\ \sum_{l=1}^M \phi_{\bar{k}_l} e^{i\bar{k}_l(z-z')} \bar{\phi}_{\bar{k}_l}^\dagger \mathcal{Y}^{-1}, & z \leq z'. \end{cases} \quad (2.10)$$

The matrix  $\mathcal{V}$  is defined by

$$\mathcal{V} = \sum_{l=1}^M H_{-l} [\phi_{k_l} e^{-ik_l} \tilde{\phi}_{k_l}^\dagger - \phi_{\bar{k}_l} e^{-i\bar{k}_l} \tilde{\phi}_{\bar{k}_l}^\dagger], \quad (2.11)$$

and the set of vectors  $\tilde{\phi}_{k_l}^\dagger$  ( $\tilde{\phi}_{\bar{k}_l}^\dagger$ ) are the duals of the set  $\phi_{k_l}$  ( $\phi_{\bar{k}_l}$ ), defined by

$$\tilde{\phi}_{k_l}^\dagger \phi_{k_h} = \tilde{\phi}_{\bar{k}_l}^\dagger \phi_{\bar{k}_h} = \delta_{lh}, \quad (2.12)$$

from which the completeness conditions follow

$$\sum_{l=1}^M \phi_{k_l} \tilde{\phi}_{k_l}^\dagger = \sum_{l=1}^M \phi_{\bar{k}_l} \tilde{\phi}_{\bar{k}_l}^\dagger = \mathcal{I}. \quad (2.13)$$

Equation (2.10) is the retarded Green's function for an infinite system. For a semi-infinite lead, it must be modified to satisfy the boundary conditions at the end of the leads. Consider first the left lead, which extends to  $z = -\infty$  and terminates at  $z = z_0 - 1$ , so that the position of the first missing slice is  $z = z_0$ . To satisfy the boundary condition that the Green's function must vanish at  $z = z_0$ , we subtract from the right-hand side of Eq. (2.10) a wave function of the form

$$\Delta_z(z', z_0) = \sum_{lh}^M \phi_{\bar{k}_h} e^{i\bar{k}_h z} \Delta_{hl}(z', z_0), \quad (2.14)$$

where  $\Delta_{hl}(z', z_0)$  is a complex matrix, determined from the condition that the Green's function vanishes at  $z_0$ , which yields

$$\begin{aligned} \Delta_z(z', z_0) &= \Delta_{z'}(z, z_0) \\ &= \sum_{l,h=1}^M \phi_{\bar{k}_h} e^{i\bar{k}_h(z-z_0)} \tilde{\phi}_{\bar{k}_h}^\dagger \phi_{k_l} e^{ik_l(z_0-z')} \tilde{\phi}_{k_l}^\dagger \mathcal{V}^{-1}. \end{aligned} \quad (2.15)$$

For the purpose of computing the scattering matrix, we shall require the Green's function of the semi-infinite left lead  $\tilde{g}_{zz'}(z_0) = g_{zz'} - \Delta_z(z', z_0)$  evaluated at the surface of the lead, namely, at  $z = z' = z_0 - 1$ . Note that in contrast with the Green's function of an infinite lead, which depends only on the difference between  $z$  and  $z'$ , the Green's function  $\tilde{g}$  of a semi-infinite lead for arbitrary  $z, z'$  is, in addition, a function of the position  $z_0$  of the first missing slice beyond the termination point of the lead. Writing  $g_L = g_{(z_0-1)(z_0-1)}(z_0)$  yields for this surface Green's function

$$g_L = \left[ \mathcal{I} - \sum_{l,h} \phi_{\bar{k}_h} e^{-i\bar{k}_h} \tilde{\phi}_{\bar{k}_h}^\dagger \phi_{k_l} e^{ik_l} \tilde{\phi}_{k_l}^\dagger \right] \mathcal{V}^{-1}. \quad (2.16)$$

Similarly, at the surface of the right lead, which extends to  $z = +\infty$ , the corresponding surface Green's function is

$$g_R = \left[ \mathcal{I} - \sum_{l,h} \phi_{k_h} e^{ik_h} \tilde{\phi}_{k_h}^\dagger \phi_{\bar{k}_l} e^{-i\bar{k}_l} \tilde{\phi}_{\bar{k}_l}^\dagger \right] \mathcal{V}^{-1}. \quad (2.17)$$

The expressions (2.16) and (2.17), when used in conjunction with Eq. (2.8) form a versatile method of determining the lead Green's functions, without the need to perform

$k$ -space integrals or contour integration. As a consequence of translational invariance of the infinite system, the surface Green's functions are independent of the position of the surface  $z_0$ . Furthermore, as noted below, in the case of different vectors  $\phi_k$ , corresponding to the same real  $k$ , the current operator is not diagonal. Hence, it is convenient to perform a unitary rotation in such a degenerate subspace to ensure the unitarity of the  $S$  matrix.

## B. The effective Hamiltonian of the scattering region

Given the Hamiltonian of a scattering region and a matrix of couplings to the surfaces of external leads, the Green's function of the scatterer plus leads can be computed from Dyson's equation (2.21). For structures, such as those in Fig. 1 with a quasi-one-dimensional geometry and a Hamiltonian which is block tridiagonal (i.e., of a finite range), this task can be made more efficient by first projecting out the internal degrees of freedom of the scatterer (2.18). This would yield an effective Hamiltonian involving only those degrees of freedom which are at the surfaces of the external leads. Then, secondly, one can calculate the Green's function for the whole system (2.21), comprising the scatterer and the leads, and evaluate transport coefficients of interest. In the literature, depending on the context or details of implementation, this procedure is sometimes referred to as the "recursive Green's-function technique" or the "decimation method," but is no more than an efficient implementation of Gaussian elimination.<sup>14</sup>

Consider a scatterer composed on  $N - 2M$  degrees of freedom. Then the Hamiltonian for the scatter plus semi-infinite leads is of the form  $H = H_L + H_R + \tilde{H}$ , where  $H_L, H_R$  are the Hamiltonians of the left and right isolated leads and  $\tilde{H}$  a  $N \times N$  Hamiltonian describing the scattering region and any additional couplings involving surface sites of the leads induced by the presence of the scatterer. The aim of the decimation (i.e., recursive Green's function) method is to successively eliminate the internal degrees of freedom of the scatterer, which we label  $i, i = 1, 2, \dots, N - 2M$ , to yield a  $(2M) \times (2M)$  effective Hamiltonian  $H_{\text{eff}}$ . After eliminating the degree of freedom  $i = 1$ ,  $\tilde{H}$  is reduced to a  $(N - 1) \times (N - 1)$  matrix with elements

$$H_{ij}^{(1)} = \tilde{H}_{ij} + \frac{\tilde{H}_{i1} \tilde{H}_{1j}}{E - \tilde{H}_{11}}. \quad (2.18)$$

Repeating this procedure  $l$  times, we obtain the "decimated" Hamiltonian at  $l$ th order

$$H_{ij}^{(l)} = H_{ij}^{(l-1)} + \frac{H_{il}^{(l-1)} H_{lj}^{(l-1)}}{E - H_{ll}^{(l-1)}}, \quad (2.19)$$

and after  $N - 2M$  such steps, an effective Hamiltonian  $H_{\text{eff}} = H^{N-2M}$  of the form

$$H_{\text{eff}}(E) = \begin{pmatrix} H_L^*(E) & H_{LR}^*(E) \\ H_{RL}^*(E) & H_R^*(E) \end{pmatrix}. \quad (2.20)$$

In this expression,  $H_L^*(E)$  [ $H_R^*(E)$ ] describes intrasurface couplings involving degrees of freedom belonging to the sur-

face of the left (right) lead and  $H_{LR}^*(E) = H_{LR}^*(E)^\dagger$  describes the effective coupling between the surfaces of the left and the right leads.

Since the effective Hamiltonian is energy dependent, this procedure is a particularly useful method when one wishes to compute the Green's function at a given energy. It is also very efficient in the presence of short range interactions, because only matrix elements involving degrees of freedom coupled to the decimated one are redefined. Since the problem now involves only  $(2M) \times (2M)$  matrices, it is straightforward to obtain the surface Green's function for the whole system (i.e., the scattering region attached to the semi-infinite leads) by solving the Dyson's equation

$$G(E) = [g(E)^{-1} - H_{\text{eff}}(E)]^{-1}, \quad (2.21)$$

where

$$g(E) = \begin{pmatrix} g_L(E) & 0 \\ 0 & g_R(E) \end{pmatrix}, \quad (2.22)$$

with  $g_L$  and  $g_R$  given by Eqs. (2.16) and (2.17).

### C. The scattering matrix and transport coefficients

To extract transport coefficients from the Green's function, we generalize the method described in Ref. 14 [in particular see Eq. (A26) of Ref. 14] to the case of nonorthogonal scattering channels. For a system of Hamiltonian  $H$ , the  $S$  matrix is defined to connect incoming to outgoing propagating states in the external leads. If  $k$  ( $k'$ ) are real incoming (outgoing) wave vectors of energy  $E$ , then an incident plane wave in one of the leads with longitudinal wave vector  $k$ , will scatter into outgoing plane waves  $k'$  with amplitudes  $s_{k'k}(E, H)$ . If all plane waves are normalized to unit flux by dividing by the square root of their group velocities then, provided the plane wave basis diagonalizes the current operator in the leads, the outgoing flux along channel  $k'$  is  $|s_{k'k}(E, H)|^2$ , and  $S$  will be a unitary matrix. If  $H$  is real, then  $S$  will be symmetric. More generally, time reversal symmetry implies the property  $s_{k'k}(E, H) = s_{kk'}(E, H^*)$ . Evidently, if  $k, k'$  belong to the left (right) lead, then one finds the *reflection* coefficients from  $r_{k'k} = s_{k'k}$  ( $r'_{k'k} = s_{k'k}$ ). If, however,  $k$  and  $k'$  belong to left and right leads, respectively, one finds the *transmission* coefficients  $t_{k'k} = s_{k'k}$  ( $t'_{k'k} = s_{k'k}$ ).

To find the transport coefficients for the system in Fig. 2, consider the probability current for an electron in the Bloch state (2.3)

$$J_k = n_{k_\perp} v_{k_\perp}, \quad (2.23)$$

where  $n_{k_\perp}$  is the probability of finding an electron in a slice and  $v_{k_\perp}$  is the corresponding group velocity. It follows that the vector

$$\psi_z = \frac{1}{\sqrt{v_k}} e^{ikz} \phi_k, \quad (2.24)$$

is normalized to a unit flux. To compute the group velocity we note that if  $|\psi_k\rangle$  is an eigenstate of Eq. (2.1), whose projection onto slice  $z$  is  $\psi_z$ , then

$$v_k = \frac{1}{\hbar} \frac{\partial}{\partial k} \langle \psi_k | H | \psi_k \rangle = \frac{1}{\hbar} \frac{\partial}{\partial k} [\phi_k^\dagger (H_0 + H_1 e^{ik} + H_{-1} e^{-ik}) \phi_k] \quad (2.25)$$

$$= \frac{i}{\hbar} \phi_k^\dagger (H_1 e^{ik} - H_{-1} e^{-ik}) \phi_k, \quad (2.26)$$

where the last step follows from Eq. (2.4) and the normalization of  $\phi_k$ .

It can be shown that the states (2.24) diagonalize the current operator only if they correspond to the distinct  $k$  values. In the case of degenerate  $k$ 's, the current is in general non-diagonal. Nevertheless, it is always possible to define a rotation in the degenerate subspace for which the current operator is diagonal. When the degeneracy is encountered, we assume that such a rotation has been performed. With this convention, the current carried by a state of the form

$$\psi_z = \sum_l a_l \frac{e^{ik_l z}}{\sqrt{v_l}} \phi_{k_l}, \quad (2.27)$$

is simply given by  $\sum_l |a_l|^2$ .

It is now straightforward to generalize the analysis of Ref. 14 to the case of nonorthogonal scattering channels. Consider first an infinite periodic structure, whose Green's function is given by Eq. (2.10). For  $z \geq z'$ , by operating on  $g_{zz'}$  from the right with the following projector:

$$P_l(z') = \mathcal{V} \phi_{k_l} \frac{e^{ik_l z'}}{\sqrt{v_l}}, \quad (2.28)$$

yields the normalized plane wave (2.24). Similarly, by acting on the Green's function  $g_{zz'}(z_0)$  of a semi-infinite left lead terminating at  $z_0$ , one obtains for  $z \geq z'$ ,  $z_0 \geq z$ , an eigenstate of a semi-infinite lead arising from a normalized incident wave along a channel  $k_l$ .

Thus the operator  $P_l(z')$  and its left-going counterpart  $\bar{P}_l(z')$  allow us to project out wave functions from the Green's function of a given structure. For example, if  $G_{zz'}$  is the retarded Green's function for a scattering region sandwiched between two perfect leads whose surfaces are located at the points  $z=0$  and  $z=L$ , then, for  $z' \leq 0$ , the projected wave function is of the form

$$\psi_z = \begin{cases} \frac{e^{ik_l z}}{\sqrt{v_l}} \phi_{k_l} + \sum_h \frac{r_{hl}}{\sqrt{v_h}} e^{ik_h z} \phi_{k_h}, & z \leq 0, \\ \sum_h \frac{t_{hl}}{\sqrt{v_h}} e^{ik_h z} \phi_{k_h}, & z \geq L, \end{cases} \quad (2.29)$$

where  $r_{hl} = r_{\bar{k}_h, k_l}$ ,  $t_{hl} = t_{k_h, k_l}$  are the reflection and the transmission coefficients associated with an incoming state from the left. In particular, for  $z=L$ ,  $z'=0$ , one obtains

$$\sum_h \frac{t_{hl}}{\sqrt{v_h}} e^{ik_h L} \phi_{k_h} = G_{L0} P_l(0) \quad (2.30)$$

and hence

TABLE I. Lattice constants of the metals considered in the calculation.

Metal	Lattice constant (Å)
Co	3.55
Ni	3.52
Cu	3.61
Ag	4.09
Pd	3.89
Au	4.08
Pt	3.92

$$t_{hl} = \tilde{\phi}_{k_h}^\dagger G_{L0} \mathcal{V} \phi_{k_l} \sqrt{\frac{v_h}{v_l}} e^{-ik_h L}. \quad (2.31)$$

Since the right-hand side of Eq. (2.31) involves only the surface Green's function of Eq. (2.21) the transmission coefficients (and by analogy all other transport coefficients) are thus finally determined. Since the above analysis is valid for any choice of the Hamiltonians  $H_0$  and  $H_1$ , this approach is indeed very general.

### III. RESULTS FOR Co AND Ni BASED MULTILAYERS

Using the technique developed above, we have studied transport properties of multilayers formed from Co and Ni as magnetic layers and several  $3d$ ,  $4d$ , and  $5d$  transition metals as nonmagnetic spacer layers. All of these metals have a fcc lattice structure with the following lattice constants listed in Table I.

It is clear that Co and Ni have a good lattice match with Cu, while for the other metals the lattice mismatch is large and may introduce strain and defects at the interface. The latter produces an additional scattering at the interfaces, neglected in our present calculations. Nevertheless, we will show that large values of the GMR ratio can be obtained, in agreement with experimental values, suggesting that CPP GMR is a bulk effect, whose main features are contained in a ballistic quantum description of the conductance with an adequate band structure. Below we model all the metals by an  $spd$  tight-binding Hamiltonian with nearest-neighbor couplings, whose parameters are chosen to fit the band structure evaluated from first-principles calculations.<sup>18</sup> The hopping parameters at the heterojunctions between materials have been approximated by a geometric mean of the corresponding pure metal values. It is worth noting that different averaging procedures used to obtain the hopping coefficients in the heterojunctions yield small changes in the calculated conductance of the multilayers. Nonetheless, a more realistic approach to the heterojunctions between different metals, based on *ab initio* calculations, would be useful to clarify the role of coupling across the interfaces in such structures.

#### A. Density of electronic states (DOS) and conductance of the pure metals

We begin our analysis by examining the DOS and conductance of the pure metals. Since the Hamiltonians include  $spd$  hybridization, angular momentum states are not eigenstates of the system. However, in order to understand the

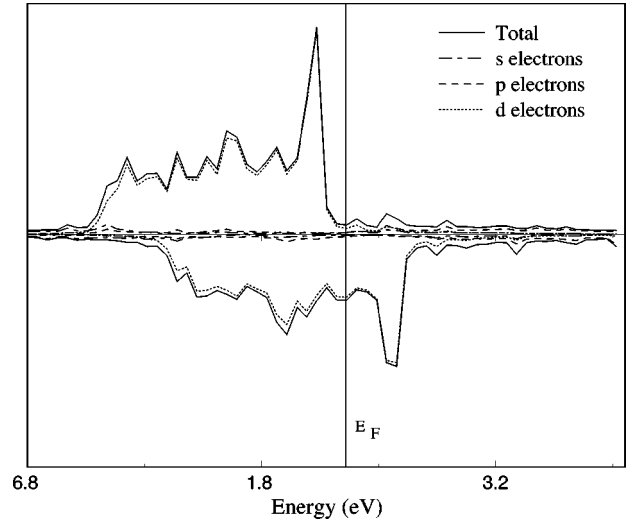


FIG. 3. DOS for pure Co. The vertical line denotes the position of  $E_F$  that is chosen to be 0 eV.

relative role of the angular character interband and intraband scattering, it is useful to project the DOS and conductance onto an angular momentum basis. We will label as an  $s$ -like electron (and similarly for the  $p$  and  $d$  electrons) an electron whose  $s$  component  $|\langle s | \psi \rangle|^2$  of the wave function  $|\psi\rangle$  is much larger than the  $p$  and  $d$  components.

The DOS's for the two spin sub-bands of Co and Ni are very similar, and we show, as an example, the Co DOS in Fig. 3. As in all the  $d$  transition metals, the DOS is formed from a localized  $d$  band embedded in nearly parabolic  $s$  and  $p$  bands. The width of the bands is roughly the same in Co and Ni, as well as the position of the majority band with respect to the Fermi energy. In both materials, the Fermi energy lies just above the edge of the majority  $d$  band, while the minority band is almost rigidly shifted with respect to the majority band towards higher energies, the shift being larger in Co than in Ni. In both the minority bands of Co and Ni the Fermi energy lies well within the  $d$  band and the DOS is completely dominated by the  $d$  electrons. A rough estimate of the mismatch between the minority  $d$  bands of Co and Ni can be obtained from the on-site energies of the  $d$  electrons in the minority band. As shown in Table II, the difference between the on-site energies of the  $d$  minority electrons in Co and Ni is about 0.7 eV and it corresponds to the relative shift of the bands (the on-site energies shown in the table are chosen in order to have the Fermi energy  $E_F = 0$ ).

The conductance of pure Co and Ni is determined solely by the DOS. For majority electrons at the Fermi energy, the

TABLE II. On-site energies used in the calculations.

Metal	$E_s$ (eV)	$E_p$ (eV)	$E_d$ majority (eV)	$E_d$ minority (eV)
Co	5.551	14.025	-2.230	-0.660
Ni	4.735	11.850	-2.114	-1.374
Cu	2.992	10.594	-2.746	-2.746
Ag	2.986	9.127	-4.650	-4.650
Pd	5.764	11.457	-2.050	-2.050
Au	0.329	10.081	-3.823	-3.823
Pt	1.849	11.523	-2.614	-2.614

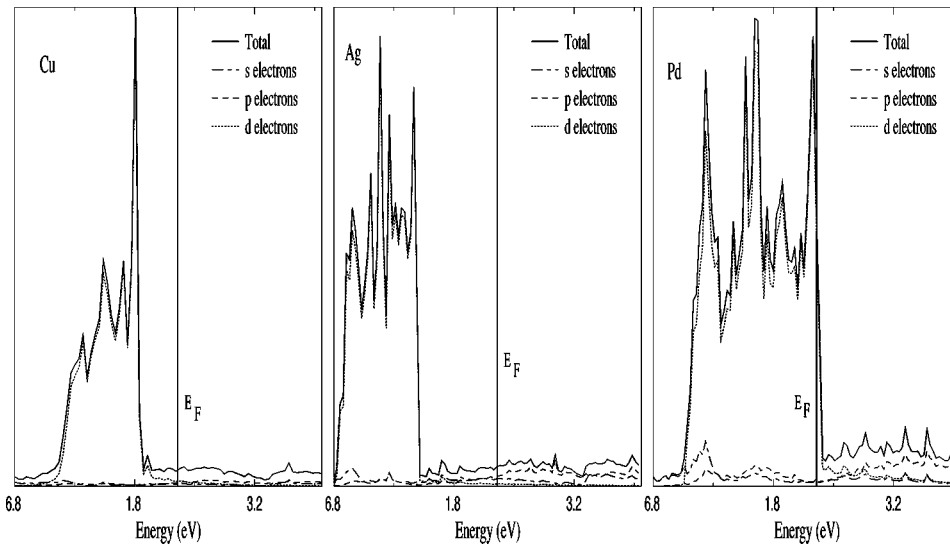


FIG. 4. DOS for pure Cu, Ag, and Pd. The vertical lines denote the position of the Fermi energy, which is chosen to be  $E_F=0$ .

current is carried by the  $s$ ,  $p$ , and  $d$  electrons, which give almost equal contributions. On the other hand, the current carried by minority electrons is completely dominated by the  $d$  electrons, with the contributions from  $s$  and  $p$  electrons being no larger than 10% of the total. If we neglect the relative shift in energies of the minority bands, the Ni and Co conductances possess the same qualitative features and, since the effective mass is proportional to the inverse of the band width, we find that the current carried by majority electrons is formed from a mixture of light  $s$  and  $p$  electrons and heavy  $d$  electrons, whereas the minority-electron current is carried almost entirely by heavy  $d$  electrons.

Now consider the nonmagnetic  $3d$ ,  $4d$ , and  $5d$  transition metals with fcc lattices. A glance at the DOS of these materials reveals three types of band structure: (i) the DOS closely matches the DOS of the majority spin sub-band of Co and Ni (e.g., Cu and Au), (ii) the DOS has only  $sp$  components at the Fermi energy, with the  $d$  component highly suppressed (as in Ag), and (iii) the DOS is composed of an almost pure  $d$  component at the Fermi energy (e.g., for Pd and Pt). Examples of each of these cases are given in Fig. 4, which shows the DOS of Cu, Ag, and Pd and in Fig. 5, which displays the corresponding conductances.

As we shall see below for ballistic structures, the mismatch between the bands of the magnetic and nonmagnetic metals forming the multilayer is the key feature which determines the conductance. Moreover, although the positions of the  $s$  and  $p$  bands are the same for both spins, for  $d$  electrons the two spin sub-bands possess a different mismatch at the interface and therefore this mismatch (potential step for  $d$  electrons at the interface) largely determines the magnitude of CPP GMR.

In addition to the above generic features, the on-site energies of the  $s$  bands of Au and Pt are small compared with those of Ni and Co. In the Co/Au and Co/Pt multilayers, this may induce strong scattering of the  $s$  electrons, resulting in a strong suppression of the  $s$ -electron contribution to the total conductance. This effect should be weaker in the Pt-based than in the Au-based multilayers, because a DOS of Platinum has mainly  $d$  character at the Fermi energy, which means that the Co/Pt multilayers will be sensitive to the effect of the large  $s$ -band mismatch only through the hybridization of the  $s$  and  $d$  bands at the Fermi energy.

Figure 5 shows how these three distinct DOS characteristics are reflected in the conductances of the normal metals and give rise to three different scenarios for charge transport:

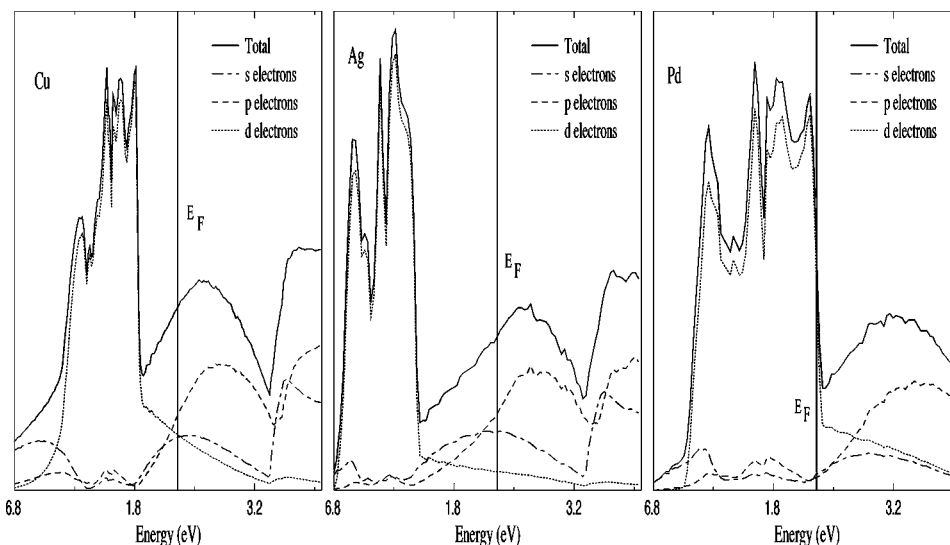


FIG. 5. The conductance for pure Cu, Ag, and Pd. The vertical lines denote the Fermi energy  $E_F=0$ .

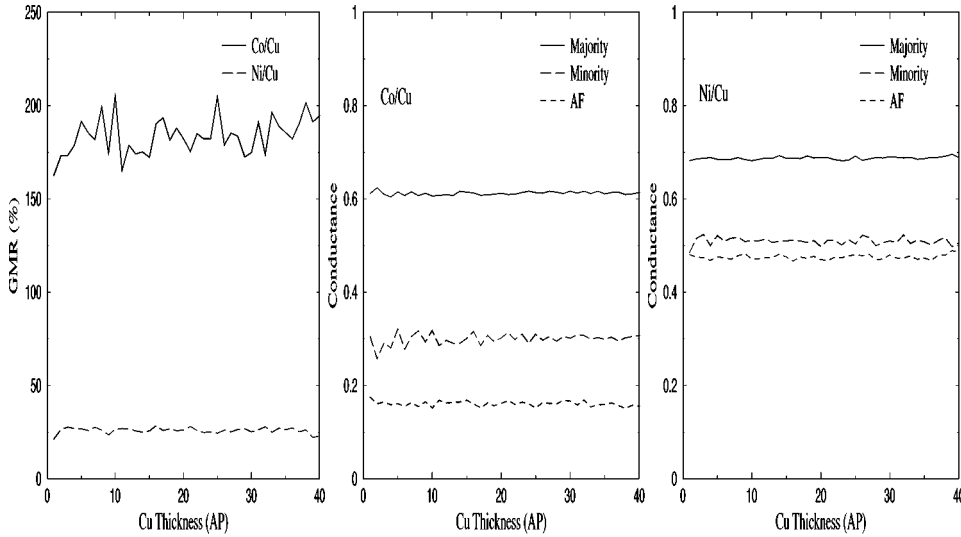


FIG. 6. GMR and spin conductance for Co/Cu and Ni/Cu systems as a function of the Cu layers thickness. The first graph is the GMR, the second is the conductance for the Co/Cu system normalized to the conductance of pure Cu, and the third is the conductance of the Ni/Cu system with the same normalization. To evaluate the conductance in units of  $\Omega^{-1} \text{m}^{-2}$ , these data should be multiplied by the conversion factor  $f_{\text{Cu}} = 0.61 \times 10^{15}$ .

(i) the contributions to the current from  $s$ ,  $p$ , and  $d$  electrons are almost equal (e.g., in Cu and Au), (ii) the current has a strong  $sp$  character (e.g., in Ag), and (iii) the current has a strong  $d$  character (e.g., Pd and Pt).

These different characteristics of the current carriers in the nonmagnetic metals give rise to another important source of interface scattering. Since the majority spins in the magnetic metals are mainly  $sp$  electrons with light effective masses and the minority spins are  $d$  electrons with heavy effective masses, it is clear that, depending on the choice of nonmagnetic metal, different spin-dependent interband scattering must occur at the interfaces. For example in the Co/Ag system, a majority spin propagates in Co as a mixture of  $s$ ,  $p$ , and  $d$  electrons, whereas in Ag it has mainly an  $sp$  character. This means that an electron in the Ag, whose spin is in the same direction of the magnetization, can enter Co as an  $sp$  electron without the need for strong interband scattering. On the other hand, if its spin points in the opposite direction, it will undergo an interband scattering because in the minority band the electron must propagate as a  $d$  electron. Moreover the interband scattering involves final states with a large DOS, and hence a scattering is expected to be strong.

The above observations suggest that the key mechanisms affecting transport are (i) a strong band mismatch and (ii) a strong interband scattering. The best GMR multilayers must be able to maximize electron propagation in one of the two spin bands and to minimize it in another one. To achieve this result, the high conduction spin band should have a small band mismatch and weak interband scattering at the heterojunctions, while the low conduction band should have a large band mismatch and strong interband scattering.

### B. A comparison between Co-based and Ni-based multilayers

To clarify how the spin polarization of the magnetic material affects the properties of the GMR multilayers, we begin by examining GMR in Cu-based multilayers, in which the magnetic metals are either Ni or Co. All the multilayers consist of ten bilayers of the form  $A/\text{Cu}$  where  $A$  is Co or Ni, attached to two semi-infinite Cu leads. The Fermi energy is fixed by the semi-infinite leads which is taken as zero. After calculating the different spin conductances in the ferromagnetic and antiferromagnetic configurations, the GMR ratio is

obtained from Eq. (1.1). In all our calculations the current flows in the (110) crystalline direction and the structures are translationally invariant within the layers. Below we consider  $8100 k_{\parallel}$  points ( $90 \times 90$ ) in the plane of the layers. We have estimated that the GMR ratio calculated with  $2 \times 10^4 k_{\parallel}$  points on average differs by  $\sim 3\%$ , from that calculated using

$$8100 k_{\parallel} \text{ points} \left( \frac{\text{GMR}(8100) - \text{GMR}(2 \times 10^4)}{\text{GMR}(8100)} \sim 3\% \right).$$

Since the oscillations of the GMR ratio with respect to the layer thicknesses are larger than  $3\%$ , the choice of  $8100 k_{\parallel}$  points allows us to investigate the oscillating behavior of the conductance and the GMR, and is a good compromise between the accuracy of the calculation and the required computer time. Initially we fix the magnetic layer thickness to five atomic planes, and calculate the conductance and GMR as a function of the Cu layer thickness.

We shall normalize the conductance by dividing it by the conductance of a single spin in the pure metallic leads, which is a natural choice for the present work. For results shown in Fig. 6 it means the normalization to one half of the total Cu conductance, because of a spin degeneracy.

From Fig. 6 it is clear that the Co-based multilayers show larger GMR ratios. In the ferromagnetic configuration, the majority electrons have high conductances in both cases, reflecting the good match between the majority bands of Co and Ni, and the Cu band. Moreover, the better match of the  $s$  and  $p$  majority bands of Ni with Cu, compared with those of Co, gives rise to a slightly higher conductance in majority channel for Ni than for Co. A similar argument explains the difference in the conductances of the minority channel. As we can see from Table II, the minority  $d$  band of Ni is a better match to Cu than that of Co, as indicated by the difference in the on-site energies about  $0.7 \text{ eV}$ . Hence for the minority band, the interface scattering between Co/Cu is greater for Ni/Cu. In the antiferromagnetic configuration both spins undergo the same scattering sequence, belonging alternately to the majority and to the minority bands. The total spin conductance in the antiferromagnetic configuration is found to be close to that of the minority band in the fer-

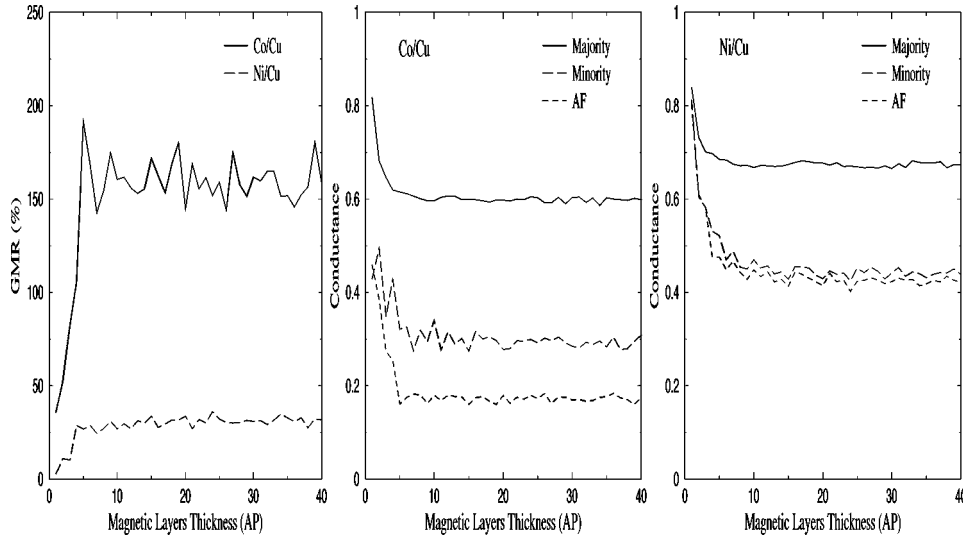


FIG. 7. GMR and spin conductance for Co/Cu and Ni/Cu systems as a function of Co and Ni layers thicknesses. The first graph is the GMR, the second is the conductance for the Co/Cu system normalized to the conductance of pure Cu, and the third is the conductance of the Ni/Cu system with the same normalization. See Fig. 6 for the conversion factor into units of  $\Omega^{-1} \text{m}^{-2}$ .

romagnetic configuration, because the minority band mismatch is larger than the majority band, and dominates the scattering.

The ratio  $R$  between the conductance ( $\Gamma$ ) of the AF configuration and of the minority band in the  $F$  configuration [ $R = \Gamma(\text{AF})/\Gamma(F \text{ minority})$ ] is  $\sim 0.6$  for Co/Cu and  $\sim 0.9$  for Ni/Cu. This difference can be understood by modeling the interface scattering through an effective step potential, whose magnitude is equal to the band mismatch, as discussed elsewhere.<sup>19</sup> The effective scattering potential in the antiferromagnetic configuration will be a sequence of high steps (for minority band) and low steps (for majority band) with respect to a common reference.

The calculated  $R$  ratios arise, because the perturbation of the minority steps due to the majority steps, is smaller in Ni/Cu than in Co/Cu. From this analysis the splitting between the two spin sub-bands in the magnetic materials is the crucial parameter leading to large GMR ratios and, since such splitting is larger in Co than in Ni, Co emerges as a natural candidate for high GMR ratio multilayers. Note that highest possible values of GMR can probably be achieved with the use of half-metallic ferromagnets with 100% spin polarization of electrons.<sup>20</sup>

Having examined the dependence of transport properties on the normal-metal layer thickness, we now examine the

dependence on the magnetic-layer thickness. For a fixed Cu layer-thickness of five atomic planes, Fig. 7 shows results for Co/Cu and Ni/Cu multilayers. A key result in this figure is that for thin magnetic layers GMR in both Ni/Cu and Co/Cu multilayers is suppressed. This can be understood in terms of an effective scattering potential. The large off-sets between the minority  $d$  bands of the different materials create an effective barrier in the  $d$  band, for channels with high transverse momentum. When the width of such a barrier is small, tunneling across the magnetic metal within the  $d$  band is possible, and this results in an enhancement of the conductance in the minority spin channel and hence in a reduction of GMR. Thus we predict a lower limit of approximately four atomic planes to the magnetic-layer thickness, in order to achieve the highest possible GMR ratio. In what follows we will only consider thicknesses larger than this value.

### C. Dependence of GMR on nonmagnetic spacer material

We now consider the dependence of GMR on the choice of nonmagnetic material in Co- and Ni-based multilayers. In all calculations we fix the Co thickness at five and ten atomic planes and vary the thickness of the nonmagnetic layers from 1 to 40 atomic planes. The material in the external leads is the same nonmagnetic material used for the multilayers (e.g.,

TABLE III. GMR ratio and GMR oscillations for different metallic multilayers.

Multilayer	GMR ratio (%)	$\Delta$ (%)	$\Delta 1$ (%)	$\Delta/\text{GMR}$ (%)	$\Delta 1/\text{GMR}$ (%)
Co <sub>5</sub> /Cu	183.7	10.0	12.4	5.4	6.7
Co <sub>5</sub> /Ag	153.7	9.5	13.1	6.1	8.5
Co <sub>5</sub> /Pd	102.0	13.9	16.7	13.7	13.4
Co <sub>5</sub> /Pt	104.1	10.9	15.6	10.5	15.0
Co <sub>5</sub> /Au	98.8	20.4	33.62	20.6	34.0
Co <sub>10</sub> /Cu	150.7	9.2	9.2	6.1	6.1
Co <sub>10</sub> /Ag	131.0	7.6	5.3	5.8	4.1
Co <sub>10</sub> /Pd	165.2	31.1	32.2	18.8	19.4
Co <sub>10</sub> /Pt	175.7	14.8	21.1	8.4	12.5
Co <sub>10</sub> /Au	138.8	20.1	26.4	14.5	17.8
Ni <sub>5</sub> /Cu	25.9	1.5	1.8	5.8	6.9
Ni <sub>5</sub> /Co <sub>5</sub>	66.1	4.1	6.6	6.2	10.0

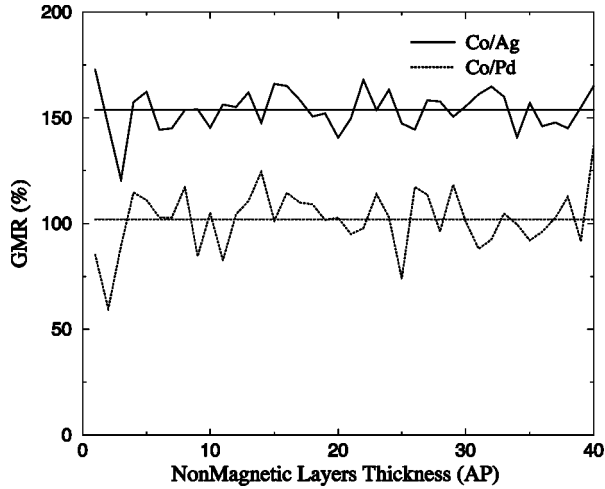


FIG. 8. GMR as a function of the nonmagnetic metal layer thickness for Co/Ag and Co/Pd. The horizontal lines denote the position of the average GMR.

Ag in Co/Ag multilayers). Table III shows the average value of the GMR ratio and the root mean square amplitude of oscillation around such value ( $\Delta$ ). To highlight the fact that GMR is an oscillatory function of the normal-metal thickness with an amplitude which decreases with increasing thickness, the table also shows the mean square oscillation calculated for nonmagnetic metal layers thicknesses between 1–10 ( $\Delta 1$ ). In the table the subscript at Co indicates the number of atomic planes of the Co layers. The penultimate row of the table shows results for the Ni/Cu system, for which we believe that no current perpendicular to planes (CPP) experimental results are currently available, even though the CIP conductance in high magnetic field has been studied.<sup>21</sup> We also show the hypothetical GMR values for Co/Ni multilayers in the last row of the table. The Schuller's group at UCSD has not observed any GMR for Co/Ni multilayers, likely because of a strong exchange coupling between the layers. From Table III it is clear that the GMR ratio results depend quite sensitively on the multilayer geometry, i.e., on the layer thicknesses. In fact the simulations with the Co thickness fixed at five atomic planes seem to

suggest that the *sp* conductors as spacer layers (Cu, Ag) result in larger GMR ratios in this case. The simulations with ten Co atomic planes show that the multilayers with *d*-electron spacers (Pd, Pt) correspond to relatively larger GMR. It is also evident that the Co based multilayers show much larger GMR ratios than the Ni based multilayers. The table also demonstrates that the conductors dominated by *d* electrons, namely, Pd and Pt, have very similar GMR ratios and amplitudes of oscillation and that Au has the largest amplitude oscillations. As examples, Fig. 8 shows plots of the GMR ratio as a function of the nonmagnetic metal layer thickness for the Co/Ag and Co/Pd systems.

In all cases (excluding Au) the oscillations are small compared with the average value of the GMR ratio, suggesting that there is an additional contribution to the long range oscillations observed experimentally. This is most likely to arise from a periodic deviation from a perfect antiferromagnetic configuration, the possibility of which is neglected in our calculations. It is important to point out that a perfect antiferromagnetic alignment of the multilayer in zero magnetic field is a consequence of the exchange coupling of the adjacent magnetic layers through the nonmagnetic layer. The strength and phase of such coupling depend critically on the Fermi surface of the nonmagnetic metal.<sup>22</sup> To the best of our knowledge no experimental data are available for the *d* conductor multilayers, for which the antiferromagnetic configuration may be difficult to achieve. In spin valves, however, such an antiferromagnetic configuration can always be obtained by tuning the coercive fields of the different magnetic layers, for instance by an appropriate choice of the spin valve geometry, or by using some magnetization pinning technique. Hence our theoretical predictions for Co/Pd and Co/Pt multilayers can, at least in principle, be tested experimentally.

The above results for the GMR ratio somewhat obscure the material dependence of the electrical conductance and with a view to comparing these with their band structures, we now present results for the conductances of the different spin channels and of the AF configuration. In the Tables IV, V, and VI we present the conductance ( $\Gamma$ ), the mean conductance oscillation ( $\Delta\Gamma$ ), their ratio ( $\Delta\Gamma/\Gamma$ ), the maximum

TABLE IV. Conductance and conductance oscillations for different metallic multilayers: majority band. The conductance of each multilayer is normalized to the conductance of the corresponding nonmagnetic metal, which composes the leads. To evaluate the conductance in units of  $\Omega^{-1} \text{m}^{-2}$ , see conversion factors in the caption to Fig. 9.

Multilayer	$\Gamma$	$\Delta\Gamma$	$\Delta\Gamma/\Gamma$ (%)	$\Delta\Gamma_{\max}$	$\Delta\Gamma_{\max}/\Gamma$ (%)
Co <sub>5</sub> /Cu	0.61	$3.76 \times 10^{-3}$	0.61	$1.17 \times 10^{-2}$	1.92
Co <sub>5</sub> /Ag	0.66	$4.10 \times 10^{-3}$	0.62	$1.24 \times 10^{-2}$	1.88
Co <sub>5</sub> /Pd	0.35	$5.32 \times 10^{-3}$	1.50	$1.52 \times 10^{-2}$	4.29
Co <sub>5</sub> /Pt	0.38	$5.01 \times 10^{-3}$	1.31	$1.87 \times 10^{-2}$	4.91
Co <sub>5</sub> /Au	0.24	$1.22 \times 10^{-2}$	4.94	$5.07 \times 10^{-2}$	20.52
Co <sub>10</sub> /Cu	0.59	$5.33 \times 10^{-3}$	0.90	$1.06 \times 10^{-2}$	1.81
Co <sub>10</sub> /Ag	0.63	$4.37 \times 10^{-3}$	0.69	$1.31 \times 10^{-2}$	2.06
Co <sub>10</sub> /Pd	0.33	$8.89 \times 10^{-3}$	2.67	$2.05 \times 10^{-2}$	6.14
Co <sub>10</sub> /Pt	0.37	$5.02 \times 10^{-3}$	1.37	$1.25 \times 10^{-2}$	3.41
Co <sub>10</sub> /Au	0.24	$1.05 \times 10^{-2}$	4.42	$3.69 \times 10^{-2}$	15.53
Ni <sub>5</sub> /Cu	0.69	$3.11 \times 10^{-3}$	0.45	$8.31 \times 10^{-3}$	1.21

TABLE V. Conductance and conductance oscillations for different metallic multilayers: minority band. The conductance of each multilayer is normalized to the conductance of the corresponding nonmagnetic metal, which composes the leads. To evaluate the conductance in units of  $\Omega^{-1} \text{m}^{-2}$ , see the caption to Fig. 9.

Multilayer	$\Gamma$	$\Delta\Gamma$	$\Delta\Gamma/\Gamma$ (%)	$\Delta\Gamma_{\text{max}}$	$\Delta\Gamma_{\text{max}}/\Gamma$ (%)
Co <sub>5</sub> /Cu	0.29	$1.19 \times 10^{-2}$	3.97	$4.21 \times 10^{-2}$	14.04
Co <sub>5</sub> /Ag	0.28	$1.15 \times 10^{-2}$	4.08	$4.01 \times 10^{-2}$	14.31
Co <sub>5</sub> /Pd	0.18	$1.23 \times 10^{-2}$	6.93	$4.13 \times 10^{-2}$	23.24
Co <sub>5</sub> /Pt	0.19	$8.54 \times 10^{-3}$	4.29	$2.51 \times 10^{-2}$	12.65
Co <sub>5</sub> /Au	0.20	$1.06 \times 10^{-2}$	5.08	$3.52 \times 10^{-2}$	16.86
Co <sub>10</sub> /Cu	0.32	$1.08 \times 10^{-3}$	3.38	$2.82 \times 10^{-2}$	8.80
Co <sub>10</sub> /Ag	0.32	$1.75 \times 10^{-2}$	5.54	$5.73 \times 10^{-2}$	18.15
Co <sub>10</sub> /Pd	0.16	$1.56 \times 10^{-2}$	9.78	$3.50 \times 10^{-2}$	21.14
Co <sub>10</sub> /Pt	0.19	$9.02 \times 10^{-3}$	4.71	$2.63 \times 10^{-2}$	13.73
Co <sub>10</sub> /Au	0.16	$9.60 \times 10^{-3}$	5.95	$2.34 \times 10^{-2}$	14.53
Ni <sub>5</sub> /Cu	0.51	$7.63 \times 10^{-3}$	1.49	$2.39 \times 10^{-2}$	4.71

of the conductance oscillations ( $\Delta\Gamma_{\text{max}}$ ) and its ratio with the mean conductance ( $\Delta\Gamma_{\text{max}}/\Gamma$ ), respectively for the majority electrons in the ferromagnetic configuration, the minority electrons in the ferromagnetic configuration, and both spins in the antiferromagnetic configuration. All conductances are normalized to the single-spin conductance of the nonmagnetic-metal leads. This allows us to compare the different scattering properties arising from the electronic structure of the multilayers independently of the material of the leads. It is possible to extract the values of the conductance per unit area in units of  $\Omega^{-1} \text{m}^{-2}$  by multiplying the normalized conductances by the following conversion factors  $f$ :  $f_{\text{Cu}} = 0.61 \times 10^{15} \Omega^{-1} \text{m}^{-2}$ ,  $f_{\text{Ag}} = 0.45 \times 10^{15} \Omega^{-1} \text{m}^{-2}$ ,  $f_{\text{Au}} = 0.47 \times 10^{15} \Omega^{-1} \text{m}^{-2}$ ,  $f_{\text{Pd}} = 0.73 \times 10^{15} \Omega^{-1} \text{m}^{-2}$ ,  $f_{\text{Pt}} = 0.83 \times 10^{15} \Omega^{-1} \text{m}^{-2}$ . Note that the absolute values of conductance per unit area are consistent with *ab initio* calculations for infinite superlattices in the ballistic regime.<sup>7</sup>

Tables IV–VI illustrate that, with the exception of Au, materials belonging to the same class have similar normalized conductances. For Cu and Ag the majority (minority) band is a high (low) transmission band, leading to a large GMR ratio for such materials. The majority bands of these

two materials match that of Co and there is little interband scattering (even less in Ag where the electrons at the Fermi energy are completely *sp*). By contrast, the minority carriers are subject to a large scattering potential due to a difference between the on-site energies of the *d* band. They are also subject to large interband scattering because of almost pure *d* character of the minority carriers in Co. On the other hand, for Pd and Pt, which are *d* metals, both sub-bands are subject to high scattering albeit for different reasons. The on-site energies of the majority band of Co, Pd, and Pt are roughly the same, ensuring a good band match. It is worth noting that the width of the *d* majority band of Co is associated with hybridization of *s*, *p*, and *d* electrons, while the Pd and Pt bands are mainly *d*-like. Hence, a strong inter-band scattering is present in the majority band of Co/Pd and Co/Pt superlattices. By contrast, the minority band is *d*-like in Co, Pd, and Pt, but there is a significant difference in the on-site energies, resulting in a large effective potential step at the interface.

The Au/Co multilayers lie somewhat outside the above picture, because even though the *d* band resembles that of Ag, the on-site energies of the *s* and *p* bands are considerably

TABLE VI. Conductance and conductance oscillations for different metallic multilayers: AF configuration. The conductance of each multilayer is normalized to the conductance of the corresponding nonmagnetic metal, which composes the leads. To evaluate the conductance in units of  $\Omega^{-1} \text{m}^{-2}$ , see conversion factors in the caption to Fig. 9.

Multilayer	$\Gamma$	$\Delta\Gamma$	$\Delta\Gamma/\Gamma$ (%)	$\Delta\Gamma_{\text{max}}$	$\Delta\Gamma_{\text{max}}/\Gamma$ (%)
Co <sub>5</sub> /Cu	0.16	$5.33 \times 10^{-3}$	3.31	$1.35 \times 10^{-2}$	8.40
Co <sub>5</sub> /Ag	0.18	$6.71 \times 10^{-3}$	3.62	$2.34 \times 10^{-2}$	12.68
Co <sub>5</sub> /Pd	0.13	$7.98 \times 10^{-3}$	6.04	$1.52 \times 10^{-2}$	15.00
Co <sub>5</sub> /Pt	0.14	$6.87 \times 10^{-3}$	4.81	$2.28 \times 10^{-2}$	16.01
Co <sub>5</sub> /Au	0.11	$1.25 \times 10^{-2}$	10.85	$5.49 \times 10^{-2}$	47.45
Co <sub>10</sub> /Cu	0.18	$6.40 \times 10^{-3}$	3.51	$1.62 \times 10^{-2}$	8.94
Co <sub>10</sub> /Ag	0.21	$5.10 \times 10^{-3}$	2.46	$1.06 \times 10^{-2}$	5.17
Co <sub>10</sub> /Pd	$9.41 \times 10^{-2}$	$1.09 \times 10^{-2}$	11.62	$3.15 \times 10^{-2}$	33.45
Co <sub>10</sub> /Pt	0.10	$4.77 \times 10^{-3}$	4.69	$1.43 \times 10^{-2}$	14.12
Co <sub>10</sub> /Au	$8.40 \times 10^{-2}$	$6.95 \times 10^{-3}$	8.27	$1.66 \times 10^{-2}$	19.77
Ni <sub>5</sub> /Cu	0.47	$4.85 \times 10^{-3}$	1.02	$1.38 \times 10^{-2}$	2.91

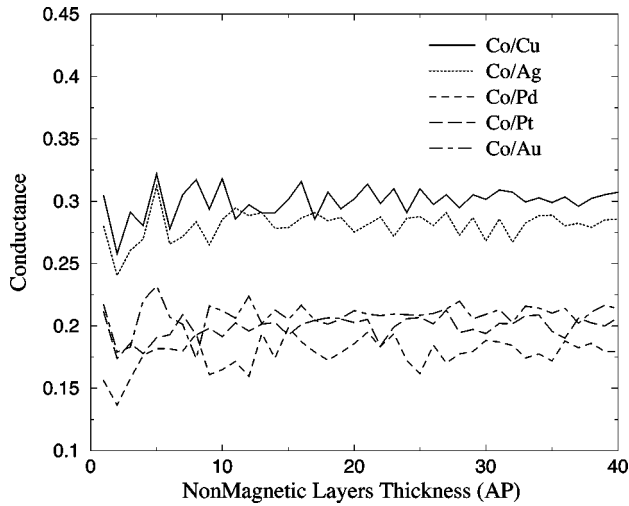


FIG. 9. Conductance of the minority spin electrons as a function of the nonmagnetic layers thickness. The conductance of each multilayer is normalized to the conductance of the corresponding nonmagnetic metal, which composes the leads. To evaluate the conductance in units of  $\Omega^{-1} \text{ m}^{-2}$ , these data should be multiplied by the following conversion factors:  $f_{\text{Cu}}=0.61 \times 10^{15}$ ,  $f_{\text{Ag}}=0.45 \times 10^{15} \Omega^{-1} \text{ m}^{-2}$ ,  $f_{\text{Au}}=0.47 \times 10^{15} \Omega^{-1} \text{ m}^{-2}$ ,  $f_{\text{Pd}}=0.73 \times 10^{15} \Omega^{-1} \text{ m}^{-2}$ ,  $f_{\text{Pt}}=0.83 \times 10^{15} \Omega^{-1} \text{ m}^{-2}$ .

smaller than the corresponding bands in Co. This means that strong scattering occurs in the  $s$  and  $p$  bands and since the  $s$  and  $p$  electrons of Au carry most of the current, there is a strong suppression of the conductance in all spin channels. From the above tables, we see that the Co/Au system possesses a low conductance in all the spin channels and in the antiferromagnetic configuration.

Finally we note that, compared with the majority spin channel, the oscillations are larger in the minority spin channel and in the antiferromagnetic configuration. This suppression of oscillations in the former occurs because of the better band matching in the majority band. In Fig. 9 we show the conductance of the minority band as a function of the nonmagnetic layers thickness, for all the materials studied.

The oscillations that we observe never exceed 20% of their mean value (except for the Co/Au system) and they are larger for smaller thicknesses. This is substantially smaller than the observed values for Co/Ni system.<sup>23,24</sup> The difference may in part be related to scattering on disorder, always present in experimental systems, and to a simplicity of a tight-binding model that we used. In addition, actual mag-

netic configuration in those systems can be somewhat different as compared to an ideal one that we considered. It is interesting to note that, generally, materials with small conductances ( $\Gamma < 0.25$  using the usual normalization for conductances) have larger oscillations, because low conductances indicate strong scattering potentials and, hence, larger fluctuations. A qualitative picture of these conductance oscillations has been presented in another publication,<sup>19</sup> where the above quantitative results are compared with a simple Kronig-Penney model.

#### IV. CONCLUSION

First, we have developed a completely general Green's function technique for elastic spin-dependent transport calculations, which (i) scales linearly with a system size and (ii) allows straightforward application to general tight-binding ( $spd$  in the present work) Hamiltonians. This technique can be applied to unrestricted studies of different systems, including tunneling spin valves<sup>20,25,26</sup> and magnetic multilayers with superconducting leads. The formulas (2.16) and (2.17) for the surface Green's functions of external leads are the central result of the first part. Explicit general expressions for the Green's functions enable us to avoid using a small imaginary part in energy.

Secondly, we have presented an extensive study of transport in magnetic multilayers in CPP geometry in the limit of large coherence length. Ni and Co were considered as materials for magnetic layers and several  $3d$ ,  $4d$ , and  $5d$  metals as nonmagnetic spacers. Key parameters have been identified as controlling a giant magnetoresistance in those systems. These are the character of electronic states at the Fermi level and a mismatch in relevant band edges across interfaces. We have found that, in accordance with experiment,<sup>23,24</sup> there are oscillations in the conductance as a function of both magnetic and spacer layer thicknesses. The magnitude of the calculated oscillations is, however, smaller than those observed experimentally. Some reasons for this behavior have been identified and they deserve further study. A semiquantitative analysis of the conductance oscillations is presented elsewhere.<sup>19</sup>

#### ACKNOWLEDGMENTS

The authors wish to acknowledge Professor Ivan Schuller for valuable and useful discussions. This work was supported by the EPSRC and the EU TMR Program.

\*Electronic address: sanvito@dera.gov.uk

†Electronic address: c.lambert@lancaster.ac.uk

‡Electronic address: alexb@hpl.hp.com

<sup>1</sup>M.N. Baibich, J.M. Broto, A. Fert, F. Nguyen Van Dau, F. Petroff, P. Etienne, G. Creuzet, A. Friederich, and J. Chazelas, Phys. Rev. Lett. **61**, 2472 (1988); G. Binasch, P. Grünberg, F. Saurenbach, and W. Zinn, Phys. Rev. B **39**, 4828 (1989).

<sup>2</sup>R.E. Camley and J. Barnas, Phys. Rev. Lett. **63**, 664 (1989).

<sup>3</sup>W.P. Pratt, Jr., S.-F. Lee, J.M. Slaughter, R. Loloee, P.A. Schroeder, and J. Bass, Phys. Rev. Lett. **66**, 3060 (1991); M.A.M. Gijs, S.K.J. Lenczowski, and J.B. Giesbers, *ibid.* **70**, 3343 (1993).

<sup>4</sup>N.F. Mott, Adv. Phys. **13**, 325 (1964).

<sup>5</sup>S.S.P. Parkin, Phys. Rev. Lett. **67**, 3598 (1991).

<sup>6</sup>K.M. Schep, P.J. Kelly, and G.E.W. Bauer, Phys. Rev. Lett. **74**, 586 (1995).

<sup>7</sup>K.M. Schep, P.J. Kelly, and G.E.W. Bauer, Phys. Rev. B **57**, 8907 (1998), and references therein.

<sup>8</sup>M. Büttiker, Y. Imry, R. Landauer, and S. Pinhas, Phys. Rev. B **31**, 6207 (1985).

<sup>9</sup>M.A.M. Gijs and G.E.W. Bauer, Adv. Phys. **46**, 285 (1997).

<sup>10</sup>W.H. Butler, X.G. Zhang, D.M.C. Nicholson, and J.M. MacLaren, Phys. Rev. B **52**, 13 399 (1995).

<sup>11</sup>E.Yu. Tsymlal and D.G. Pettifor, Phys. Rev. B **54**, 15 314

- (1996). Note that their numerical result of a high sensitivity of CPP transport in spin valves to a spin asymmetry of the electronic density of states has been shown to contradict experimental data: K. Mizushima, T. Kinno, T. Yamauchi, and K. Tanaka, *IEEE Trans. Magn.* **33**, 3500 (1997).
- <sup>12</sup>M.D. Stiles, *J. Appl. Phys.* **79**, 5805 (1996).
- <sup>13</sup>J. Mathon, *Phys. Rev. B* **55**, 960 (1997).
- <sup>14</sup>C.J. Lambert, V.C. Hui, and S.J. Robinson, *J. Phys.: Condens. Matter* **5**, 4187 (1993).
- <sup>15</sup>B. Kramer and A. MacKinnon, *Rep. Prog. Phys.* **56**, 1469 (1993).
- <sup>16</sup>A. Oguri, Y. Asano, and S. Maekawa, *J. Phys. Soc. Jpn.* **61**, 2652 (1992).
- <sup>17</sup>T.N. Todorov, E.Y. Tsymlal, and D.G. Pettifor, *Phys. Rev. B* **54**, 12 685 (1996).
- <sup>18</sup>D.A. Papaconstantopoulos, *Handbook of the Band Structure of Elemental Solids* (Plenum, New York, 1986).
- <sup>19</sup>S. Sanvito, C.J. Lambert, J.H. Jefferson, and A.M. Bratkovsky, *J. Phys.: Condens. Matter* **10**, L691 (1998).
- <sup>20</sup>A.M. Bratkovsky, *Phys. Rev. B* **56**, 2344 (1997).
- <sup>21</sup>H. Sato, T. Matsudai, W. Abdul-Razzaq, C. Fierz, and P.A. Schroeder, *J. Phys.: Condens. Matter* **6**, 6151 (1994).
- <sup>22</sup>P. Bruno, *Phys. Rev. B* **52**, 411 (1995).
- <sup>23</sup>J.M. Gallego, D. Lederman, S. Kim, and I.K. Schuller, *Phys. Rev. Lett.* **74**, 4515 (1995).
- <sup>24</sup>D. Lederman, J.M. Gallego, S. Kim, and I.K. Schuller, *J. Magn. Magn. Mater.* **183**, 261 (1998).
- <sup>25</sup>A.M. Bratkovsky, *Appl. Phys. Lett.* **72**, 2334 (1998).
- <sup>26</sup>A.M. Bratkovsky and J.H. Nickel, *J. Magn. Soc. Jpn.* **23**, 789 (1999).